Publications of the Astronomical Society of the Pacific, 130:054203 (11pp), 2018 May https://doi.org/10.1088/1538-3873/aab142

A Binary Nature of the Marginal CP Star Sigma Sculptoris

Jan Janík[1], Jiří Krtička[1], Zdeněk Mikulášek[1], Juraj Zverko[2], Olga Pintado[3], Ernst Paunzen[1], Milan Prvák[1], Jan Skalický[1], Miloslav Zejda[1], and Christian Adam[4]
[1] Department of Theoretical Physics and Astrophysics, Faculty of Science, Masaryk University Kotlářská 2, CZ-611 37 Brno, Czech Republic
honza@physics.muni.cz
[2] SK-059 60, Tatranská Lomnica 133, Slovakia
[3] Instituto Superior de Correlación Geológica, CONICET, San Miguel de Tucumán, Argentina
[4] Instituto de Astronomia, Universidad Catolica del Norte, Av. Angamos 0610, Castilla 1280 Antofagasta, Chile
Received 2017 November 13; accepted 2018 February 20; published 2018 April 2

Abstract

The A2 V star σ Scl was suspected of being a low-amplitude rotating variable of the Ap-type star by several authors. Aiming to decide whether the star is a variable chemically peculiar (CP) star, we searched for the photometric and spectroscopic variability, and determined chemical abundances of σ Scl. The possible variability was tested using several types of periodograms applied to the photometry from Long-Term Photometry of Variables project (LTPV) and *Hipparcos*. Sixty spectrograms of high signal-to-noise (S/N) were obtained and used for chemical analysis of the stellar atmosphere and for looking for spectral variability that is symptomatic for the CP stars. We did not find any signs of the light variability or prominent chemical peculiarity, that is specific for the CP stars. The only exception is the abundance of scandium, which is significantly lower than the solar one and yttrium and barium, which are strongly overabundant. As a by-product of the analysis, and with the addition of 29 further spectra, we found that σ Scl is a single-lined spectroscopic binary with orbital period of 46.877(8) d. We argue that σ Scl is not an Ap star, but rather a marginal Am star in SB1 system. The spectral energy distribution of the binary reveals infrared excess due to circumstellar material.

Key words: stars: chemically peculiar – stars: early-type – (stars:) binaries: spectroscopic – stars: variables: general – stars: individual (σ Scl) < – Stars

Online material: color figure

1. Introduction

The peculiarity of a part of the upper main-sequence stars manifests itself through enhanced spectral lines of some chemical elements and weakened lines of helium, calcium, and scandium. Even if this phenomenon has been known since the end of the nineteenth century (Maury 1897), several fundamental questions remain unanswered until now.

The peculiarity of stars with spectra classified as "Ap" or "Bp," was explained as a consequence of overabundance and a deficit of chemical elements in their atmospheres, which differ from the standard solar abundance (for example Preston 1974). It is accepted that such a phenomenon is a consequence of slow atomic diffusion or a settling in calm upper layers of these stars, then designated as chemically peculiar "CP" stars (Michaud 1970). A further key feature of the classical Ap and Bp stars are periodic changes in the strength and radial velocity of spectral lines and a weak or moderate photometric variability of the same period.

Babcock (1947) discovered a global dipolar magnetic field in the star 78 Virginis and cataloged similar stars (Babcock 1958) in which the variability of the field strength in many Ap and Bp stars–including even a reversal of magnetic polarity—was also unveiled. Stibbs (1950) introduced the "Oblique Rotator" model, representing a rigidly rotating star with non-coincident magnetic and rotational axes. Due to the uneven distribution of chemical elements on the stellar surface, the spectral and the related photometric variabilities have been easily understood. However, the expected strict relationship between the locations of spectral and photometric spots on the magnetic chemically peculiar (mCP) stars and their magnetic field geometry is documented in only a few members of the mCP stars.

Recently, Rusomarov et al. (2015) showed that surface abundance maps of HD 24712 are inconsistent with the predictions of the current theory of atomic diffusion in the presence of magnetic fields. Krtička et al. (2007, 2009) concluded that although the agreement between the observed and computed light curves seems satisfactory, other effects such as NLTE may play a major role. Shulyak et al. (2010) summarize that the simulated light variability of ε UMa is in very close agreement with the observations; however, the theoretical variation of its β index (defined by Crawford & Mander (1966) related to the Balmer Hβ line) is approximately one order of magnitude smaller than the observed. Krtička et al.

Table 1
Published Parameters of σ Scl (HD 6178, HIP 4852, and HR 293)

Spectral type	A2 V	Abt & Morrell (1995)
Johnson *B*	5.586 ± 0.014 mag	Høg et al. (2000)
Johnson *V*	5.501 ± 0.009 mag	Høg et al. (2000)
Strömgren *u*	7.061 ± 0.016 mag	Hauck & Mermilliod (1998)
Strömgren *v*	5.778 ± 0.013 mag	Hauck & Mermilliod (1998)
Strömgren *b*	5.549 ± 0.011 mag	Hauck & Mermilliod (1998)
Strömgren *y*	5.510 ± 0.011 mag	Hauck & Mermilliod (1998)
β	2.897 ± 0.008 mag	Hauck & Mermilliod (1998)
Ks	5.224 ± 0.017 mag	Cutri et al. (2003)
v_r	−15.4 ± 0.5 km/s	Gontcharov (2006)
$v_{rot} \sin i$	82.1 ± 1.2 km/s	Díaz et al. (2011)
Distance	71.2 ± 1.6 pc	McDonald et al. (2017)

(2013) show that neither maximum overabundance of helium and silicon on the surface of the low-amplitude rotating variable CP star HD 64740 do not cause a substantial light variability.

For this study, we selected a bright star, σ Scl (HR 293), which is labeled in the SIMBAD database as an α^2 Canum Venaticorum- (ACV) type star. All published parameters of σ Scl are listed in Table 1. This group of variable stars is known to have distinctive photometric variability with an amplitude of up to a tenth of magnitude (Hümmerich et al. 2016). However, while Rufener & Bartholdi (1982) observed a variability with an amplitude of 0.06 mag in *V* filter, the revised version of the Geneva catalogue by Rufener (1988) claimed a smaller amplitude. De Rosa et al. (2014) included σ Scl in the Volume-limited A-STar (VAST) survey and reported its duplicity.

In this study, we review all available photometric observations. We also obtained a series of high-resolution, high signal-to-noise ratio (S/N) spectra to analyse the spectral line intensity variability and duplicity.

2. Photometric Variability

The star was observed within the years 1988–1993 in the Strömgren photometric system in the frame of the Long-Term Photometry of Variables project (LTPV; see Sterken (1983, 1986); Manfroid et al. (1991a, 1991b); Sterken et al. (1993)), in which σ Scl served as a comparison star *to* α Scl. In total, 1560 individual *uvby* measurements were published by Manfroid & Renson 1994, who confirmed the weak variability of σ Scl. They also indicated a few possible periods, with a most likely one $P = 2\overset{d}{.}36975(20)$, while $P = 1\overset{d}{.}37675(10)$ could be its alias.

We searched for a possible periodic variability using the LTPV data (1560 individual measurements) and H_p measurements by *Hipparcos* satellite (98 measurements; ESA 1998). The amplitude spectrum for photometric measurements bands *y, Hp, b, v, u*, do not show any pattern of apparent periodicity expected in the case of rotationally modulated variability (see Figure 1). The maximum amplitude peaks, as a rule, do not reach the level of those ones expected in pure random scatter of the signal. This level was computed by the shuffle method mentioned and described in Paunzen et al. (2013) and Mikulášek et al. (2015) for particular photometric bands. At the same time, we evaluated the statistical significance of the dominant peaks in individual photometric bands by the bootstrapping test, and found that no peak in the studied amplitude spectrum exceeds the significance of 20% (Mikulášek et al. 2015). Consequently, the accuracy of photometric measurements we have at our disposal does not allow us to find any statistically approved periodical variability. Particularly, no one from periodograms cited in Mikulášek et al. (2015), especially Periodogram with Modulated Amplitude, Robust S/N Periodogram, and Classical Lomb-Scargle Periodogram, indicate any of the periods mentioned by Manfroid & Renson (1994) (see also Figure 1).

3. Spectroscopic Variability

As a next step, we investigated the spectroscopic characteristics of σ Scl.

3.1. Observations

The observations were performed with four different echelle spectrographs. First, we used the high dispersion echelle spectrograph FEROS ($R = 48\,000$) attached to the 2.2 MPG/ESO telescope at La Silla Observatory (ESO) in Chile. We collected 60 spectra during two observational runs (34 spectra in 2011 and 26 in 2012); these spectra are listed in Table 2. Each individual spectrum has an integrating time 600 s reaching $S/N \approx 500$ with the exception of spectra for HJD = 2455776.76378-2455776.96153, which have half of the exposure time resulting in $S/N \approx 250$. The second instrument was the high dispersion echelle spectrograph GIRAFFE ($R = 23{,}000$) attached to the 1.9-m telescope at South African Astronomical Observatory (SAAO). We obtained three spectra during two nights in 2011. Each individual spectrum has an integrating time of 1200 s reaching S/N ≈ 130.

The third and fourth echelle spectrographs were REOSC ($R = 8{,}600$; 10 spectra) and high dispersion EBASIM ($R = 31{,}000$; 16 spectra) attached to the Jorge Sahade 2.15-m telescope at El Leoncito Observatory (CASLEO) in Argentina. The exposure times and S/N are listed in Table 2.

The data were reduced with the standard IRAF[5] routines. The spectra were bias-corrected and flat-fielded. We used the Th-Ar-Ne comparison spectrum for a precise wavelength calibration, which was sensed through a second fiber

[5] IRAF is distributed by NOAO, which is operated by AURA, Inc., under cooperative agreement with the National Science Foundation.

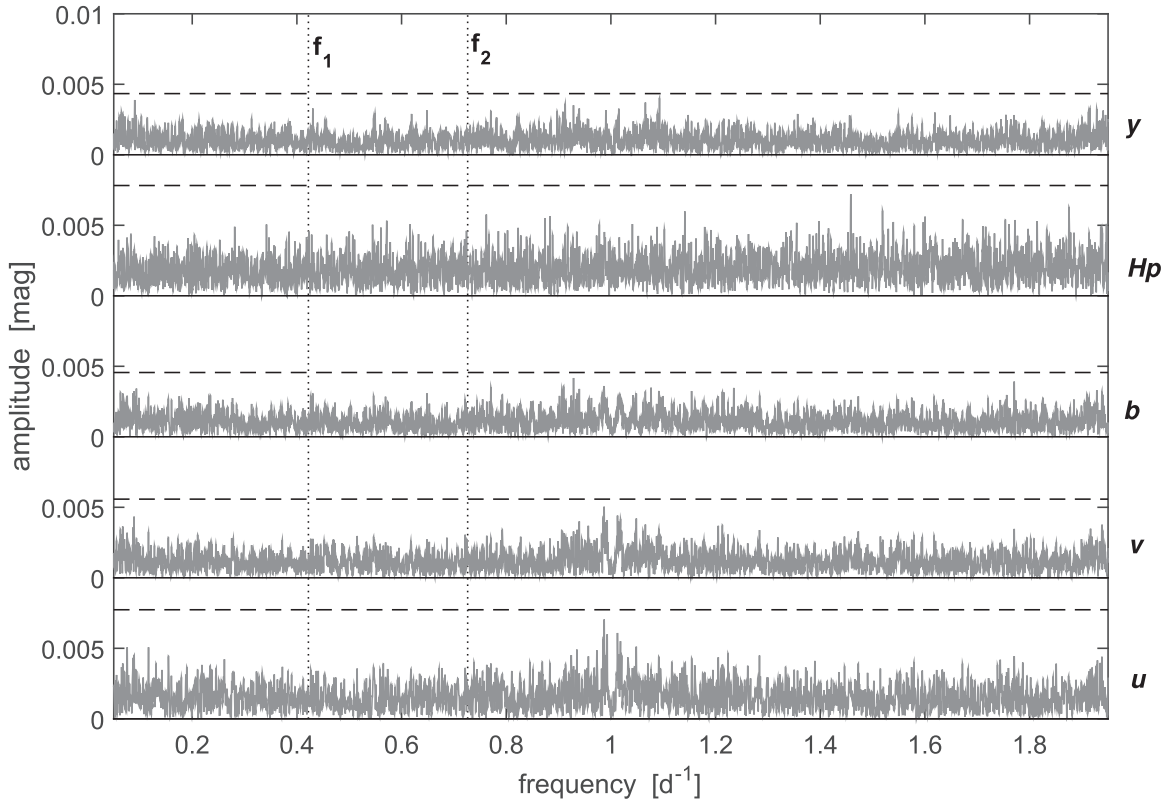

Figure 1. Amplitude spectrum of light variations of σ Scl in *u, v, b, y*, and *Hp* colors for the frequencies from 0.05 to 1.95 d^{-1}. There are no statically significant frequency peaks, except the double around the frequency of 1 sidereal day, apparent in *v* and *u*, that are the artifacts of the strong sampling of ground-based observations and imperfect detrending of *uv* data. The vertical dotted lines denote the frequencies f_1 and f_2 of variability mentioned in Manfroid & Renson (1994). The dashed lines express the mean level of the maximum peak if there is no periodic signal in measurements.

simultaneously with the spectrum of the star through the first fiber in case for FEROS spectra. For the other instruments, we used calibration Th-Ar spectra which were measured before and after the stellar spectrum. We used also IRAF (task *imexam*) for S/N measurement of normalized spectra at wavelengths where maximum signal was obtained.

3.2. Stellar Parameters

The effective temperature and surface gravity values listed in Table 3 were derived using the codes UVBYBETA (Moon & Dworetsky 1985) and TEFFLOGG (Smalley & Dworetsky 1995) using the values for *uvbyβ* from Table 1.

The evolutionary tracks for solar metallicity ([Z] = 0.014) from Bressan et al. (2012) and the above-mentioned astrophysical parameters yield an age of about 500 Myr for σ Scl.

3.3. Line Profile and Radial Velocity Variability

We investigated a possible presence of line profile variations as one of characteristic attributes of variable A-type stars. Smalley et al. (2017) investigated the pulsational behaviour of Am stars. There are δ Scuti, γ Doradus, and hybrid types found among Am stars. They conclude that δ Scuti type pulsations are mostly confined to the effective temperature range $6900 < T_{\rm eff} < 7600$ K, whereas γ Doradus stars are cooler than 7500 K. Our target is outside the blue edge of the classical instability strip given the estimated $T_{\rm eff}$ and log g values. We would therefore not expect to find pulsation within the limits of our data set.

We used for searching of line profile variations the temporal variance spectrum technique (TVS), devised by Fullerton et al. (1996). We calculated the self-TVS using the last night of FEROS data (HJD 56159). For two spectral lines in region 4400–4500 Å Ti II 4443.801 Å and Mg II 4481.327 Å and two ions Sr II 4215.519 Å, Ba II 4934.076 Å, we obtained a negative result (see Figure 2).

We also used TVS for spectra averaged over individual nights. We co-added individual shifted spectra (correcting for orbital motion) and used the first spectrum as zero point. We found again no significant signal.

We measured the individual radial velocity for each of the 89 spectra (see Table 2) by means of a cross-correlation function (CCF) using the theoretical spectrum (described in Section 3.4) as a template (Zverko et al. 2007). We processed each spectral

Table 2
List of Spectra Obtained Using FEROS@La Silla (A), GIRAFFE@SAAO (B), REOSC@CASLEO (C), and EBASIM@CASLEO (D). HJD is the Mean Heliocentric Julian Date Reduced by 2,450,000. Phase φ is Calculated According T_0 and P from Table 4

HJD	φ	In.	Reg.[nm]	τ [s]	S/N	$v_{\rm rad}$ [km s^{-1}]	HJD	φ	In.	Reg.[nm]	τ [s]	S/N	$v_{\rm rad}$ [km s^{-1}]
5775.890	0.4087	A	370–920	600	500	−0.99 ± 0.92	6157.927	0.5585	A	370–920	600	500	−5.87 ± 0.73
5775.916	0.4093	A	370–920	600	500	−0.98 ± 0.69	6158.805	0.5772	A	370–920	600	500	−6.04 ± 0.78
5775.940	0.4098	A	370–920	600	500	−0.96 ± 0.84	6158.861	0.5784	A	370–920	600	500	−6.20 ± 0.77
5776.762	0.4273	A	370–920	300	250	−1.66 ± 0.86	6158.914	0.5796	A	370–920	600	500	−6.30 ± 0.78
5776.778	0.4277	A	370–920	300	250	−1.74 ± 0.87	6158.929	0.5799	A	370–920	600	500	−6.24 ± 0.75
5776.794	0.4280	A	370–920	300	250	−1.61 ± 0.82	6159.642	0.5951	A	370–920	600	500	−6.93 ± 0.70
5776.809	0.4283	A	370–920	300	250	−1.57 ± 0.70	6159.697	0.5963	A	370–920	600	500	−6.88 ± 0.65
5776.825	0.4287	A	370–920	300	250	−1.50 ± 0.75	6159.722	0.5968	A	370–920	600	500	−6.83 ± 0.63
5776.840	0.4290	A	370–920	300	250	−1.48 ± 0.78	6159.747	0.5973	A	370–920	600	500	−6.97 ± 0.74
5776.855	0.4293	A	370–920	300	250	−1.56 ± 0.81	6159.772	0.5979	A	370–920	600	500	−6.97 ± 0.70
5776.870	0.4296	A	370–920	300	250	−1.64 ± 0.90	6159.797	0.5984	A	370–920	600	500	−6.79 ± 0.69
5776.885	0.4300	A	370–920	300	250	−1.23 ± 0.73	6159.822	0.5989	A	370–920	600	500	−6.73 ± 0.63
5776.900	0.4303	A	370–920	300	250	−1.44 ± 0.77	6159.847	0.5995	A	370–920	600	500	−6.98 ± 0.78
5776.914	0.4306	A	370–920	300	250	−1.43 ± 0.65	6159.872	0.6000	A	370–920	600	500	−6.76 ± 0.70
5776.930	0.4309	A	370–920	300	250	−1.37 ± 0.79	6159.888	0.6003	A	370–920	600	500	−6.97 ± 0.72
5776.945	0.4312	A	370–920	300	250	−1.50 ± 0.75	6159.903	0.6007	A	370–920	600	500	−6.89 ± 0.66
5776.960	0.4316	A	370–920	300	250	−1.52 ± 0.82	6159.919	0.6010	A	370–920	600	500	−6.94 ± 0.65
5777.718	0.4477	A	370–920	600	500	−1.86 ± 0.78	6159.935	0.6013	A	370–920	600	500	−7.06 ± 0.73
5777.744	0.4483	A	370–920	600	500	−1.86 ± 0.76	7173.910	0.2319	C	536–782	1800	100	−2.32 ± 1.90
5777.770	0.4488	A	370–920	600	500	−1.67 ± 0.73	7200.847	0.8065	D	483–685	900	90	−17.83 ± 1.17
5777.794	0.4494	A	370–920	600	500	−1.94 ± 0.76	7200.860	0.8068	D	483–685	900	90	−17.28 ± 1.25
5777.819	0.4499	A	370–920	600	500	−1.97 ± 0.87	7201.900	0.8290	D	483–685	900	90	−19.95 ± 1.41
5777.845	0.4504	A	370–920	600	500	−1.95 ± 0.83	7201.911	0.8292	D	483–685	900	90	−19.89 ± 1.28
5777.870	0.4510	A	370–920	600	500	−1.88 ± 0.78	7204.904	0.8931	D	399–568	1800	90	−20.53 ± 0.86
5779.722	0.4905	A	370–920	600	500	−3.18 ± 0.92	7205.859	0.9134	D	399–568	1800	90	−21.29 ± 0.83
5779.747	0.4910	A	370–920	600	500	−3.20 ± 0.78	7584.874	0.9987	C	477–632	1200	300	−14.74 ± 1.14
5779.771	0.4915	A	370–920	600	500	−2.95 ± 0.71	7585.824	0.0190	C	477–632	1200	300	−17.14 ± 1.32
5779.785	0.4918	A	370–920	600	500	−3.08 ± 0.76	7585.883	0.0203	C	477–632	1200	300	−14.47 ± 1.32
5779.812	0.4924	A	370–920	600	500	−2.98 ± 0.81	7586.824	0.0403	C	477–632	1200	300	−15.34 ± 1.47
5779.840	0.4930	A	370–920	600	500	−3.18 ± 0.79	7586.864	0.0412	C	477–632	1200	300	−10.65 ± 1.55
5779.865	0.4935	A	370–920	600	500	−3.08 ± 0.79	7587.818	0.0615	C	477–632	1200	300	−16.46 ± 1.34
5779.895	0.4942	A	370–920	600	500	−3.18 ± 0.84	7587.858	0.0624	C	477–632	1200	300	−13.22 ± 1.48
5779.914	0.4946	A	370–920	600	500	−3.26 ± 0.86	7588.796	0.0824	C	477–632	1200	300	−20.08 ± 1.51
5779.946	0.4952	A	370–920	600	500	−3.36 ± 0.93	7588.839	0.0833	C	477–632	1200	300	−11.33 ± 1.57
5790.590	0.7223	B	418–682	1200	130	−10.00 ± 1.08	7652.744	0.4466	D	503–701	3600	90	−1.47 ± 0.65
5790.662	0.7239	B	418–682	1200	130	−13.33 ± 1.66	7652.880	0.4495	D	503–701	3600	90	−0.83 ± 0.65
5793.661	0.7878	B	418–682	1200	130	−14.47 ± 1.41	7653.690	0.4668	D	503–701	3600	90	−2.23 ± 0.98
6157.728	0.5543	A	370–920	600	500	−5.56 ± 0.65	7653.850	0.4702	D	503–701	3600	90	−2.08 ± 1.20
6157.753	0.5548	A	370–920	600	500	−5.91 ± 0.77	7655.708	0.5098	D	416–547	3600	100	−3.30 ± 0.98
6157.778	0.5553	A	370–920	600	500	−5.79 ± 0.75	7655.841	0.5126	D	416–547	3600	100	−4.69 ± 0.90
6157.815	0.5561	A	370–920	600	500	−5.86 ± 0.76	7656.654	0.5300	D	416–547	3600	100	−5.14 ± 0.87
6157.840	0.5567	A	370–920	600	500	−5.80 ± 0.67	7656.812	0.5334	D	416–547	3600	100	−4.75 ± 1.06
6157.865	0.5572	A	370–920	600	500	−5.74 ± 0.68	7658.742	0.5745	D	436–581	3600	100	−5.73 ± 0.99
6157.896	0.5579	A	370–920	600	500	−5.81 ± 0.66	7658.873	0.5773	D	436–581	3600	100	−4.79 ± 1.26
6157.911	0.5582	A	370–920	600	500	−5.77 ± 0.72							

order individually and calculated the weighted mean value for each observation. Our analysis based on inspection of 89 spectrograms from four spectrographs (see Table 2) confirmed the presence of the radial velocity variability reported in the literature (Neubauer 1930; Wilson 1953; Bond et al. 1971; Gontcharov 2006). We have found that the observed radial velocity variation is cyclic with the period $P = 46\overset{\rm d}{.}877(8)$. The course of the *RV* phase curve (see Figure 3) can be explained as the consequence of the orbital motion of the primary component bound in a spectroscopic double star with the parameters summarized in Table 4. The radial velocity curve was fitted by robust regression eliminating the influence of outliers (for details, see Mikulášek & Zejda 2013). Any photometric variability connected with the orbital period of the star have not been revealed.

To detect assumptive spectral lines of the secondary component, we subtracted the average spectrum, which we have gained as sum of all spectra shifted by radial velocity of primary

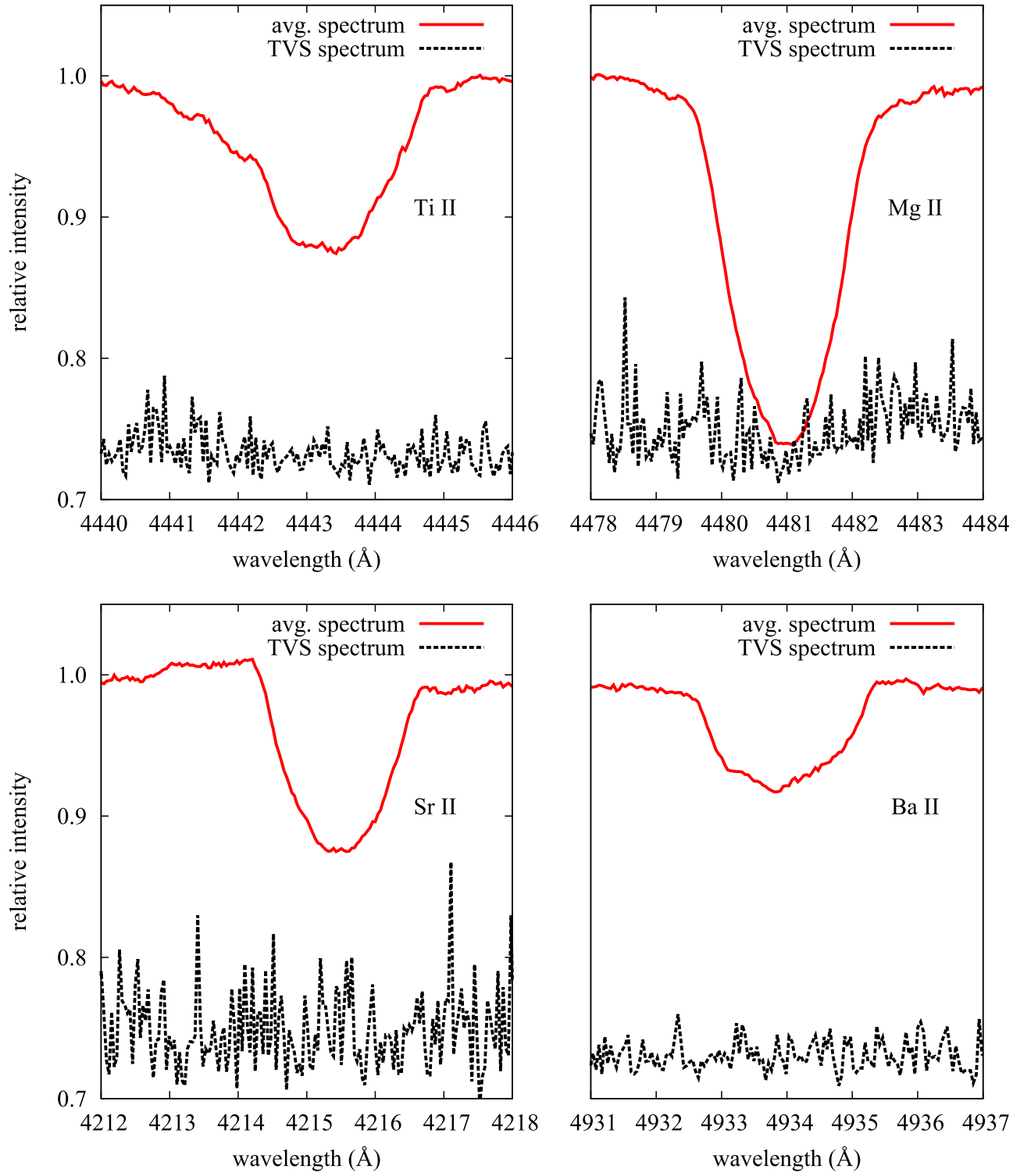

Figure 2. Averaged profiles of the spectral lines (red) Ti II 4443.801 Å (upper left), Mg II 4481.327 Å (upper right), Sr II 4215.519 Å (bottom left), and Ba II 4934.076 Å (bottom right) from night HJD 6159, and their TVS spectra (black) with no signatures of variability.
(A color version of this figure is available in the online journal.)

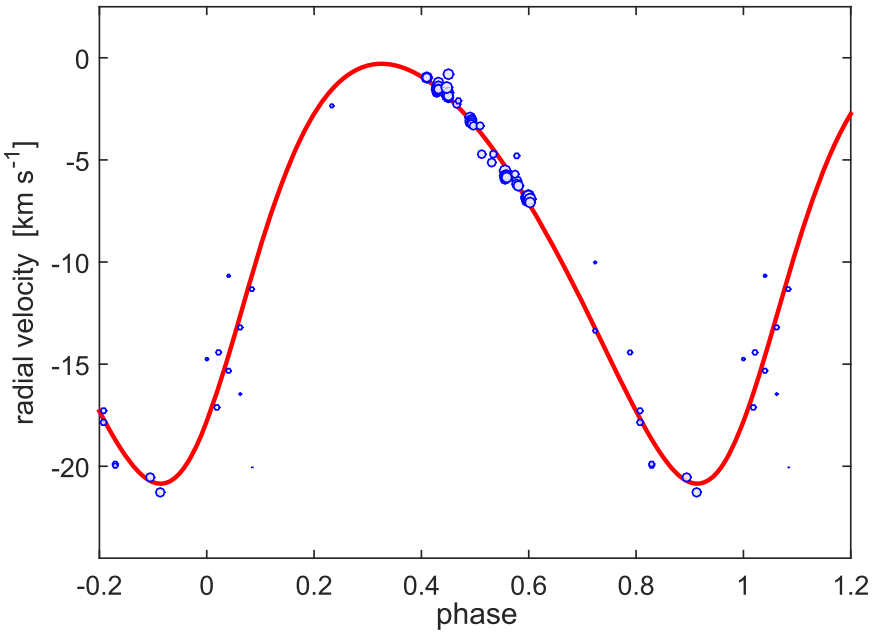

Figure 3. Radial velocity variations of σ Scl show that the star is a primary component of the single-lined spectroscopic binary with the orbital period $P = 46\overset{d}{.}877(8)$. The size of circles corresponds to the weights of individual RV measurements.
(A color version of this figure is available in the online journal.)

Table 3
Stellar Parameters of σ Scl

Effective temperature $T_{\rm eff}$	8 700 ± 125 K
Surface gravity log g (cgs)	4.11 ± 0.05

component, from each individual spectrum. Despite our best spectra were integrated to reach S/N = 500 no traces of spectral lines of the secondary component have been found. Therefore, the secondary must be either a low-luminosity star of a cool main-sequence one, or a white/brown dwarf. To specify the possible main-sequence companion closely, we estimated its upper limit of the luminosity and mass. As an example, we consider the first spectrum introduced in Table 2. Provided that a signal safely identified in a noisy continuum amounts at least 3σ, the central depth of the weakest line visible in the spectrum is $D_{\rm prim} = 0.006$ in the scale of the continuum. The spectrum of a cool main-sequence star is covered by plenty of metallic lines, the central depth of which reaches to $D_{\rm sec} = 0.9$. Then the ratio of the lights $L_{\rm prim}/L_{\rm sec} = 0.006/0.9 = 0.0067$, that results in the magnitude difference between the A2V primary and the secondary $\Delta M = 5.44$ mag. Considering that primary star has absolute magnitude $M_{\rm p}(V) = 1.3$ mag, secondary component should then have $M_{\rm s}(V) = 6.8$ mag, that corresponds to a K3V main-sequence star (Drilling & Landolt 1999). The upper mass limit of it is $\approx 0.7\,M_\odot$, and with the mass ratio of an A2V to K3V-star is $2.6/0.7 = 3.7$ and the radial velocity of the secondary in the orbital phase of the observed spectrum considered is ≈ -38 km s^{-1}. We do not identify lines of the secondary shifted with this value.

Table 4
Binary Parameters of the σ Scl System

Orbital period	$P = 46\overset{d}{.}877(8)$
JD time of periastron passage	$T_0 = 2456225.5(7)$
Numerical eccentricity	$e = 0.195(25)$
γ velocity	$\gamma = -9.2(2)$ km s^{-1}
K_1 semiamplitude	$K_1 = -10.3(3)$ km s^{-1}
Argument of the periastron	$\omega = 45(5)^\circ$

3.4. Chemical Composition

The chemical composition was derived using a χ^2 minimization of the synthetic spectra for each of the FEROS orders separately (see Figure 4). Synthetic spectra were computed using the SYNSPEC code (Hubeny & Lanz 2011), ATLAS12 model atmospheres (Bischof 2005; Castelli 2005; Kurucz 2005), and atomic data from the VALD database (Piskunov et al. 1995; Kupka et al. 1999) and also from Lanz & Hubeny (2007). The observed spectra for abundance analysis were averaged over all observations. We used a simplex method with abundances of individual chemical elements as free parameters, and we fixed stellar parameters to those given in Table 3. The final abundances of σ Scl are given in Table 5 (see also Figure 5). The abundances of individual elements were typically derived from numerous absorption lines present

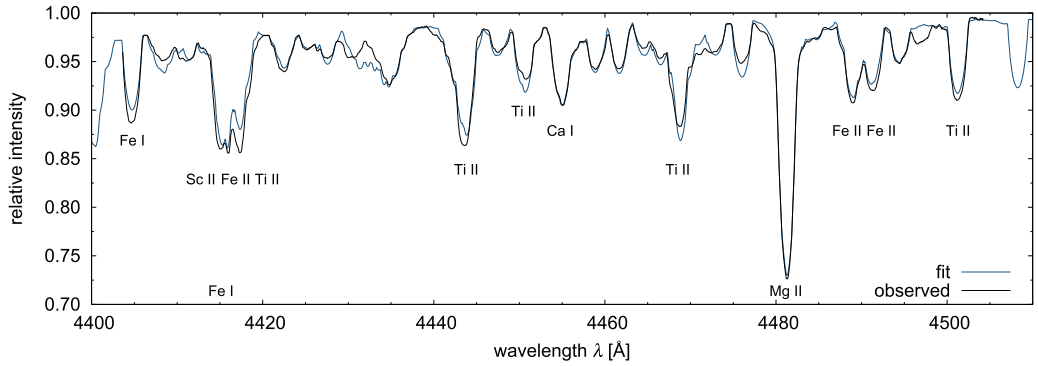

Figure 4. Comparison of the observed spectrum and the fit by the synthetic spectrum in a selected region of a FEROS spectrum.

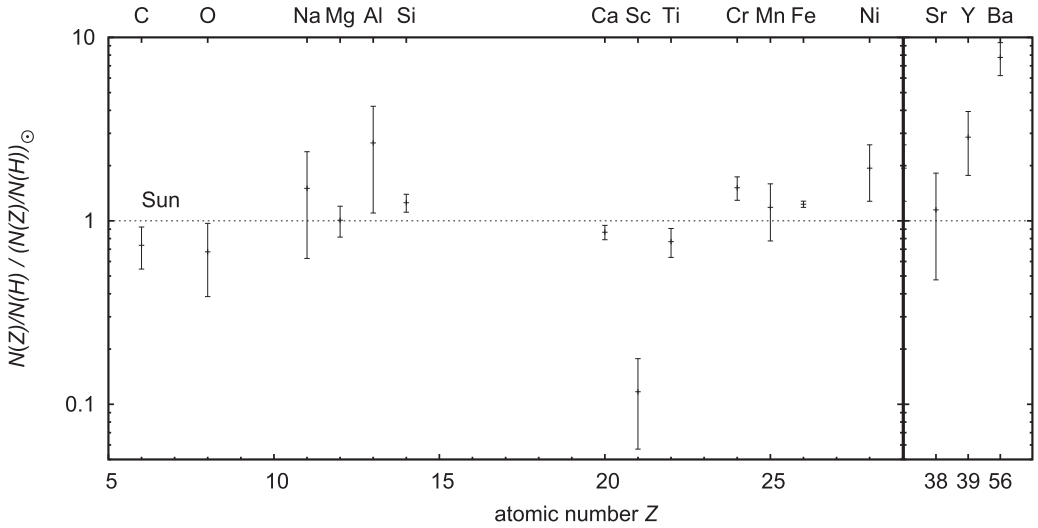

Figure 5. Derived σ Scl abundances relative to the Sun.

Table 5
Derived σ Scl Abundances

Elem.	$\log(N_{el}/N_H) + 12$		Lines	Elem.	$\log(N_{el}/N_H) + 12$		Lines
	σ Scl	Sun			σ Scl	Sun	
C	8.30 ± 0.11	8.43	5	Ti	4.83 ± 0.08	4.95	31
O	8.52 ± 0.19	8.69	4	Cr	5.82 ± 0.06	5.64	22
Na	6.42 ± 0.25	6.24	2	Mn	5.50 ± 0.15	5.43	4
Mg	7.60 ± 0.08	7.60	13	Fe	7.59 ± 0.02	7.50	∼140
Al	6.87 ± 0.25	6.45	1	Ni	6.51 ± 0.15	6.22	5
Si	7.61 ± 0.05	7.51	23	Sr	2.93 ± 0.25	2.87	1
Ca	6.28 ± 0.04	6.34	22	Y	2.65 ± 0.15	2.21	5
Sc	2.22 ± 0.22	3.15	13	Ba	3.07 ± 0.08	2.18	5

in the studied spectral range (see Table 5 for their approximate number). For most elements, the lines were present at least in three orders of FEROS spectra, and therefore we obtained at least three independent estimates of abundance for each element. The exception is Na, Al, and Sr, for which the abundances were derived from only 5683 Å and 5688 Å lines in the case of Na, 4663 Å line in the case of Al, and 4216 Å line in the case of Sr. The abundances are consistent with solar chemical composition (Asplund et al. 2009), except for a strong underabundance of scandium with a possible slight

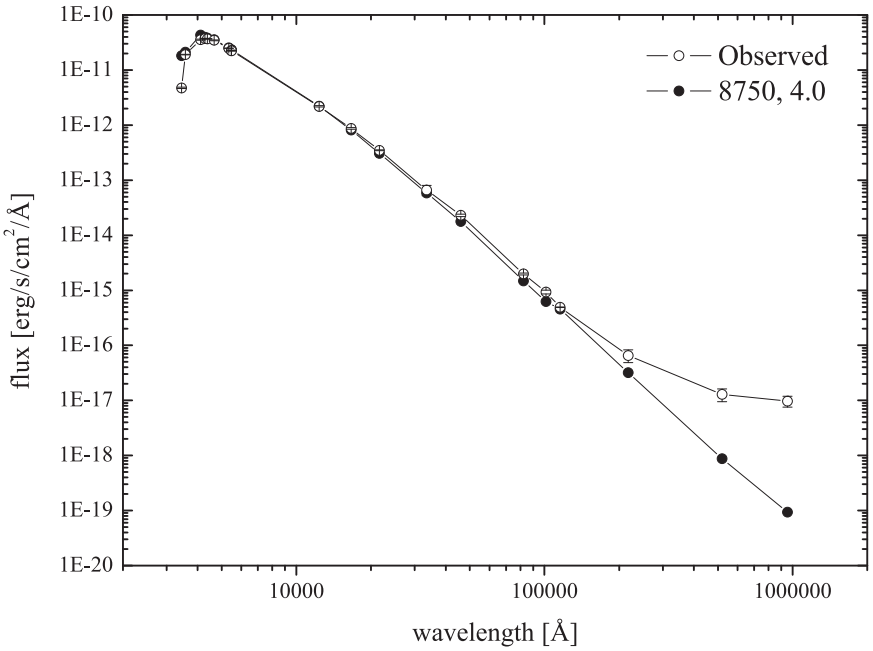

Figure 6. SED of σ Scl fitted to all available photometry and the synthetic flux from an appropriate stellar atmosphere (Castelli & Kurucz 2004). A flux excess from about 1.5 μm is evident. The infrared excess beyond 20 μm is probable due to circumstellar material.

overabundance of chromium, iron, and nickel and a strong overabundance of yttrium and barium.

This may indicate that σ Scl is a marginal Am (CP1) star. This group of chemically peculiar stars does not have a significant global magnetic field, and is preferably found in close binary systems (Adelman 1999; Hui-Bon-Hoa 2000). Almost all CP1 stars seem to be rather evolved with ages above 400 Myr (Künzli & North 1998). The derived age of σ Scl (about 500 Myr) is consistent with this conclusion.

The observed abundance pattern of CP1 stars is explained by the diffusion of elements together with the disappearance of the outer convection zone associated with the helium ionization because of gravitational settling of helium (Michaud et al. 1983). They predict a cut-off rotational velocity for such objects ($\approx$90 km s^{-1}), above which meridional circulation leads to a mixing in the stellar atmosphere. σ Scl is very close to this value, which makes it very interesting for testing the models where the transit to marginal CP1 stars takes place.

3.5. Analysis of the Spectral Energy Distribution

To put further constraints on the characteristics of the secondary component, we have investigated the spectral energy distribution (SED) of σ Scl.

For this, the VO Sed Analyzer (VOSA v5.1, Bayo et al. 2008) tool was used. All of the available photometric data were included into the fitting process. We used the synthetic flux from a standard Kurucz model (Castelli & Kurucz 2004) with $T_{\rm eff} = 8\,750$ K, $\log g = 4.0$, and solar metallicity.

Figure 6 shows the observed and synthetic fluxes. We face two different phenomena. First, there is a flux excess visible that emerges with a continuous increase from 1.5 μm. Therefore, we have calculated the difference of the fluxes and fitted a simple black body radiation curve. A temperature between 1500 and 2000 K reproduces the flux distribution well. The origin of this excess is unclear. It cannot be associated with stellar winds from the companion, because it has to be a giant with a high luminosity that is not observed.

The second, much stronger infrared excess, is visible beyond 20 μm, which can be attributed to circumstellar material within this system. It is well known that a significant number of stars in the solar neighbourhood exhibit infrared excess due to circumstellar material (Cotten & Song 2016). Most of these stars are not on the zero-age-main-sequence, but have already evolved on the main sequence. The origin of this circumstellar material is still unknown.

Herdin et al. (2016) and Chen et al. (2017) investigated the group of CP stars in the infrared region using 2MASS, IRAS, and WISE data. The latter summarized their result as follows. In the 3.4–4.6 μm region, over half of the sample have clear infrared excesses, which are possibly due to the binarity, the multiplicity, and/or the debris disk, but in the 4.6–12 μm region they have no or little infrared excess. In addition, in the 12–22 μm region, some of the targets show the infrared excesses and infrared radiation probably due to free-free emissions. In general, there is no clear picture about the nature

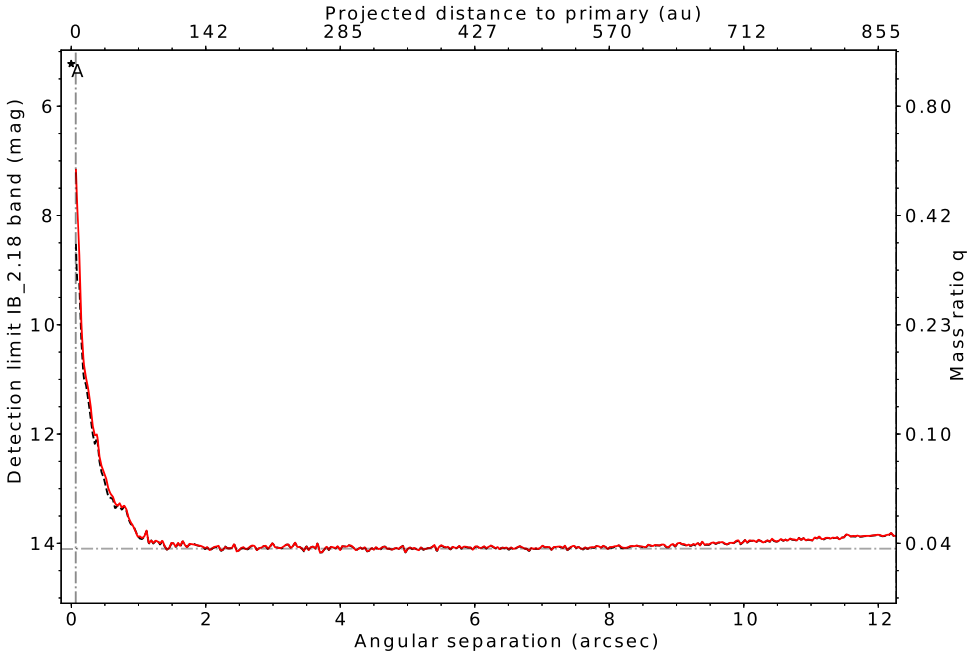

Figure 7. Dynamic range plot for σ Scl observed with NACO in 2004 November. We plot the achieved apparent magnitude (left y-axis) in the IB_2.18 filter band as function of angular (bottom x-axis) and projected separation (top x-axis), in au assuming a distance of 71.2 ± 1.6 pc (McDonald et al. 2017) could be added and adopting a K band magnitude of $Ks = 5.224 \pm 0.017$ mag (Cutri et al. 2003). The position of the primary (A) is marked with an asterisk. The measured 3σ sensitivity curve is shown as a full (red) line; objects below this line cannot be detected. The measured sensitivity curve from the PSF-subtracted image is also shown as dashed black line. The detectable mass ratios q (right y-axis) obtained from evolutionary models by Bressan et al. (2012) and the diffraction limit (vertical dash-dotted line) of the telescope are indicated as well. The background level remains constant at about 14 mag for separations outside of 1.5″ (∼0.09 $M_\odot$ at 500 Myr). No visual companion was detected within these limits.
(A color version of this figure is available in the online journal.)

of the detected infrared excesses. Here, much theoretical work is still needed to understand the possible sources.

σ Scl provides an excellent opportunity to investigate its origin and characteristics within a binary system of a very low-mass ratio.

4. NaCo and Data Reduction

Direct imaging of brown dwarfs and other cool-type stars as companions to B-type (Hubrig et al. 2001) and solar-type objects (Jenkins et al. 2010) has provided a wealth of well-constrained data. These observations have been performed using mainly adaptive optics imaging programs as part of surveys to establish the binary frequency among various star groups. We have therefore searched various data archives if such data exist for our target.

For σ Scl, high-angular resolution observations are available, taken with the Adaptive Optics camera NACO (for Nasmyth Adaptive optics system with the COude near-infrared imager and spectrograph, Rousset et al. 2003; Lenzen et al. 2003) installed at the Nasmyth B focus of the VLT/UT4 from 2001–2013.

The data set of σ Scl consists of one epoch, imaged in November 2004[6] with the IB_2.18 filter band ($\lambda = 2.18 \pm 0.06\,\mu$m) and employing the NACO S27 optics. The total integration time is 7.5 min.

For the data reduction of the NACO images, we use appropriate calibration data from the ESO data archive, i.e., darks with the same exposure time, and flats taken in the same filter and in the same night (20.11.2004 UT 3:30–3:40, HJD 53 329.647–53 329.654, orbital phase 0.22) as the science data. To reduce the imaging data, we use ESO `ECLIPSE/jitter`.[7] For each science frame, a master-dark subtraction and flat-field correction is applied, and all images are averaged using the provided shift+add procedure including measurement and subtraction of the bright background of the sky in the near-infrared.

5. Detection Limits

From the reduced the NACO IB_2.18 image of σ Scl, we measure the achieved (S/N = 3) detection limit versus angular and projected separation. To measure the dynamic range as a function of the angular separation, a 1D sensitivity curve was created using the following procedure. First, for each pixel on the detector, the distance to the previously determined position

[6] Public data from the ESO data archive, taken in ESO program 074.D-0180(A).

[7] ESO C Library for an Image Processing Software Environment.

of the central star was calculated, and the corresponding measured flux F stored. Then, n annuli of equal width were selected within which the flux values were sorted, the upper and lower 10% excluded and those values rejected that deviate by more than 3σ from the median to remove the contribution of the stars contained in the annulus from the calculation. The standard deviation of the remaining values was than used as estimate of the background noise. The resulting 3σ contrast level as a function of the angular separation is finally evaluated by comparison of the estimated background noise with the peak flux of the central star. The procedure described above was also applied to the PSF-subtracted image. However, the differences between the two resulting curves is only marginal. The main reason for this is that the main source of the noise is the photon noise, which is superimposed with the measured signal. The removal of the signal by subtraction of the PSF does not significantly change the measured residual noise, thus the computed sensitivity remains almost equal. The result is illustrated in Figure 7.

No additional source could be detected within the fully covered field of view, i.e., at angular separations smaller than about 12 arcsec (~855 au of projected separation) around the central star σ Scl. In the background-noise-limited region, a $(S/N = 3)$ detection limit of about 14 mag is reached at angular separations from σ Scl A beyond about 1.5 arcsec. At the derived age of σ Scl of about 500 Myr, this allows the detection of low-mass stellar companions with masses down to 0.09 solar masses and projected separations from σ Scl A of more than about 107 au.

6. Summary

We reanalyzed sets of photometric data available in the literature for suspected Ap star σ Scl to check them for periodicity. We do not confirm the periods indicated in the literature. We have not detected any significant light and line profile variations. The absence of line profile variations and mostly solar chemical composition support the classification of σ Scl as non-variable marginal Am main-sequence star. However, a detailed analysis of radial velocity variations revealed that σ Scl is a spectroscopic binary (SB1) with the period of 46.877(8) d. We did not find traces of the secondary component in the spectrum, but we did find a flux excess from 1.5 μm in spectral energy distribution. Yet larger flux excess is visible beyond 20 μm, and is caused probably due to circumstellar material.

This work was supported by the grants GA ČR 16-01116S, as well as MŠMT 7AMB14AT015 and 7AMB17AT030. Olga Pintado is a Visiting Astronomer, Complejo Astronómico El Leoncito, operated under agreement between the Consejo Nacional de Investigaciones Científicas y Técnicas de la República Argentina and the National Universities of La Plata, Córdoba and San Juan.

The research is based on observations obtained at the European Southern Observatory (ESO programs 087.D-0099 and 089.D-0153), at the South African Astronomical Observatory (SAAO) and at the El Leoncito Astronomical Complex (CASLEO).

ORCID iDs

Jan Janík https://orcid.org/0000-0002-6384-0184
Ernst Paunzen https://orcid.org/0000-0002-3304-5200
Miloslav Zejda https://orcid.org/0000-0001-6231-3350

References

Abt, H. A., & Morrell, N. I. 1995, ApJS, 99, 135
Adelman, S. J. 1999, MNRAS, 310, 146
Asplund, M., Grevesse, N., Sauval, A. J., & Scott, P. 2009, ARA&A, 47, 481
Babcock, H. W. 1947, ApJ, 105, 105
Babcock, H. W. 1958, ApJS, 3, 141
Bayo, A., Rodrigo, C., Barrado Y Navascués, D., et al. 2008, A&A, 492, 277
Bischof, K. M. 2005, MSAIS, 8, 64
Bond, H. E., Perry, C. L., & Bidelman, W. P. 1971, PASP, 83, 643
Bressan, A., Marigo, P., Girardi, L., et al. 2012, MNRAS, 427, 127
Castelli, F. 2005, MSAIS, 8, 25
Castelli, F., & Kurucz, R. L. 2004, arXiv:astro-ph/0405087
Chen, P. S., Liu, J. Y., & Shan, H. G. 2017, AJ, 153, 218
Cotten, T. H., & Song, I. 2016, ApJS, 225, 15
Crawford, D. L., & Mander, J. 1966, AJ, 71, 114
Cutri, R. M., Skrutskie, M. F., van Dyk, S., et al. 2003, VizieR Online Data Catalog, 2246
De Rosa, R. J., Patience, J., Wilson, P. A., et al. 2014, MNRAS, 437, 1216
Díaz, C. G., González, J. F., Levato, H., & Grosso, M. 2011, A&A, 531, A143
Drilling, J. S., & Landolt, A. U. 2002, in Allen's Astrophysical Quantities, ed. A. N. Cox (4th ed.; New York: Springer), 381
ESA 1998, The Hipparcos and Tycho Catalogs, Celestia, 2000 SP–1220
Fullerton, A. W., Gies, D. R., & Bolton, C. T. 1996, ApJ, 103, 475
Gontcharov, G. A. 2006, AstL, 32, 759
Hauck, B., & Mermilliod, M. 1998, A&AS, 129, 431
Herdin, A., Paunzen, E., & Netopil, M. 2016, A&A , 585, A67
Høg, E., Fabricius, C., Makarov, V. V., et al. 2000, A&A, 355, 27
Hubeny, I., & Lanz, T. 2011, Synspec: General Spectrum Synthesis Program, Astrophysics Source Code Library, record ascl:1109.022
Hubrig, S., Le Mignant, D., North, P., & Krautter, J. 2001, A&A, 372, 152
Hui-Bon-Hoa, A. 2000, A&AS, 144, 203
Hümmerich, S., Paunzen, E., & Bernhard, K. 2016, AJ, 152, 104
Krtička, J., Mikulášek, Z., Zverko, J., & Zižňovský, J. 2007, A&A, 470, 1089
Krtička, J., Mikulášek, Z., Henry, G. W., et al. 2009, A&A, 499, 567
Krtička, J., Janík, J., Marková, H., et al. 2013, A&A, 556, A18
Künzli, M., & North, P. 1998, A&A, 330, 651
Kupka, F., Piskunov, N., Ryabchikova, T. A., Stempels, H. C., & Weiss, W. W. 1999, A&AS, 138, 119
Kurucz, R. L. 2005, MSAIS, 8, 14
Lanz, T., & Hubeny, I. 2007, ApJS, 169, 83
Lenzen, R., Hartung, M., Brandner, W., et al. 2003, Proc. SPIE, 4841, 944
Manfroid, J., Sterken, C., Bruch, A., et al. 1991a, A&AS, 87, 481
Manfroid, J., Sterken, C., Bruch, A., et al. 1991b, ESOSR, 8, 1
Manfroid, J., & Renson, P. 1994, A&A, 281, 73
Maury, A. 1897, AnHar, 28, 1
McDonald, I., Zijlstra, A. A., & Watson, R. A. 2017, MNRAS, 471, 770
Michaud, G. 1970, ApJ, 160, 640
Michaud, G., Tarasick, D., Charland, Y., & Pelletier, C. 1983, ApJ, 269, 239
Mikulášek, Z., Paunzen, E., Netopil, M., & Zejda, M. 2015, ASPC, 494, 320

Mikulášek, Z., Žižňovský, J., Zverko, J., & Polosukhina, N. S. 2003, Contributions of the Astronomical Observatory Skalnate Pleso, 33, 29
Moon, T., & Dworetsky, M. M. 1985, MNRAS, 217, 782
Neubauer, F. J. 1930, Lick Observatory Bulletin, 15, 46
Paunzen, E., Mikulášek, Z., Poleski, R., et al. 2013, A&A, 556, A12
Jenkins, J. S., Jones, H. R. A., Biller, B., et al. 2010, A&AS, 515, A17
Piskunov, N. E., Kupka, F., Ryabchikova, T. A., Weiss, W. W., & Jeffery, C. S. 1995, A&AS, 112, 525
Preston, G. W. 1974, ARA&A, 12, 257
Rousset, G., Lacombe, F., Puget, P., et al. 2003, Proc. SPIE, 4839, 140
Rufener, F., & Bartholdi, P. 1982, A&AS, 48, 503
Rufener, F. 1988, Catalogue of Stars Measured in the Geneva Observatory Photometric System (4th ed.; Sauverny: Geneva Observatory), 39
Rusomarov, N., Kochukhov, O., Ryabchikova, T., & Piskunov, N. 2015, A&A, 573, A123
Shulyak, D., Krtička, J., Mikulášek, Z., Kochukhov, O., & Lüftinger, T. 2010, A&A, 524, A66
Smalley, B., & Dworetsky, M. M. 1995, A&A, 293, 446
Smalley, B., Antoci, V., Holdsworth, D. L., et al. 2017, MNRAS, 465, 2662
Stibbs, D. W. N. 1950, MNRAS, 110, 395
Sterken, C. 1983, Msngr, 33, 10
Sterken, C. 1986, in The Study of Variable Stars Using Small Telescopes, ed. J. R. Percy (Cambridge: Cambridge Univ. Press), 165
Sterken, C., Manfroid, J., Anton, K., et al. 1993, A&AS, 102, 79
Wilson, R. E. 1953, General Catalogue of Stellar Radial Velocities (Washington, DC: Carnegie Institute Publication)
Zverko, J., Žižňovský, J., Mikulášek, Z., & Iliev, I. K. 2007, CoSka, 37, 49